

# 21

## Element Morphing

## TABLE OF CONTENTS

	Page
§21.1. <b>Introduction</b>	21-3
§21.2. <b>Plate in Plane Stress</b>	21-4
§21.3. <b>Source Element 1: 4-node Rectangular Panel</b>	21-5
§21.3.1. Rectangular Panel Template . . . . .	21-6
§21.3.2. Morphing to Bar . . . . .	21-6
§21.3.3. Morphing to Simply Supported Beam . . . . .	21-8
§21.3.4. Morphing to Spar . . . . .	21-9
§21.4. <b>Benchmark Plane Beam Solutions</b>	21-11
§21.4.1. Symmetric Solution . . . . .	21-12
§21.4.2. Antisymmetric Elasticity Solution . . . . .	21-12
§21.4.3. Antisymmetric Timoshenko Solution . . . . .	21-13
§21.4.4. Specialization to a Rectangular Cross Section . . . . .	21-13

### §21.1. Introduction

The subject of this Chapter is a finite element fabrication, testing and optimization method called *morphing*. The word generically means “to undergo transformation” (Merriam-Webster dictionary; From Gr. morphos: shape.)

The term is nowadays used in image processing: mapping the image of an object into that of another one by means of computer software, a process sometimes endowed with animation. But the idea preceeds the computer as illustrated by well known woodcuts of M. C. Escher, e.g., Figure 21.1.

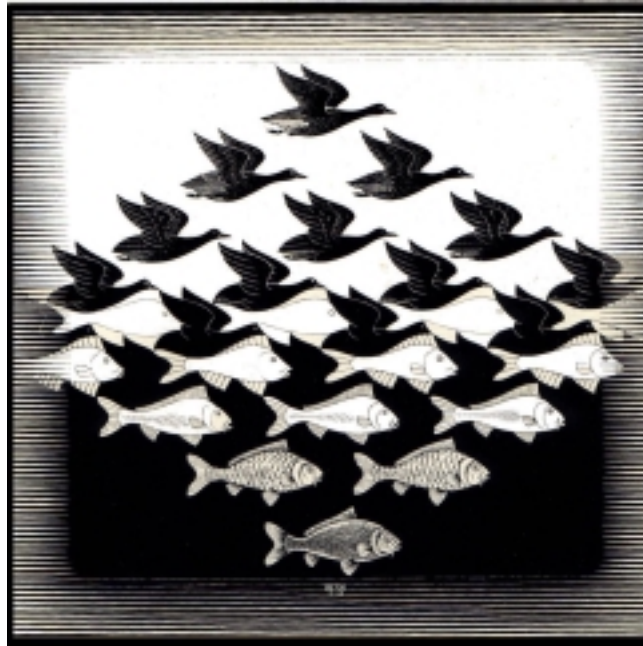


FIGURE 21.1. Escher’s Sky and Water: morphing as shape transformation.

In the finite element field, the author introduced the term *morphing* to identify the mapping of a *source element* or *macroelement* to a *target element* through kinematic constraints. (A macroelement is an assembly of few elements that may be view as a repeating mesh unit.) The target element has a smaller number of degrees of freedom and often a smaller dimensionality.

The process was originally called *retrofitting* of a parent element to a child element in []. This terminology has been changed because “child element” has been widely adopted since in adaptive mesh refinement processes.

The feedback process, which may be called “demorphing” fits appropriately under case 2 below.

What are the reasons for morphing? Improving element performance is the dominant motive. Two cases may be considered:

*Improving the source.* The source model contains adjustable parameters that survive in the target element. Improving the performance of the latter may yields values for those parameters, which are fed back.

*Deriving special elements.* The source element is fixed. Morphing is used to produced functionally specialized instances; for example a solid shell element from a general isoparametric brick. The

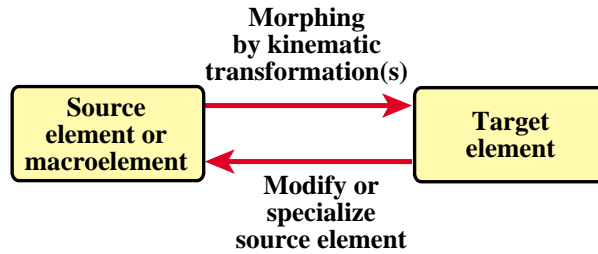


FIGURE 21.2. Element morphing and demorphing processes.

transformation may introduced free parameters in the target. These parameters are chosen to improve the performance of the target element. In turn this may pose constraints in the transformation. The process is best explained through specific examples that convey the scope of what can be accomplished.

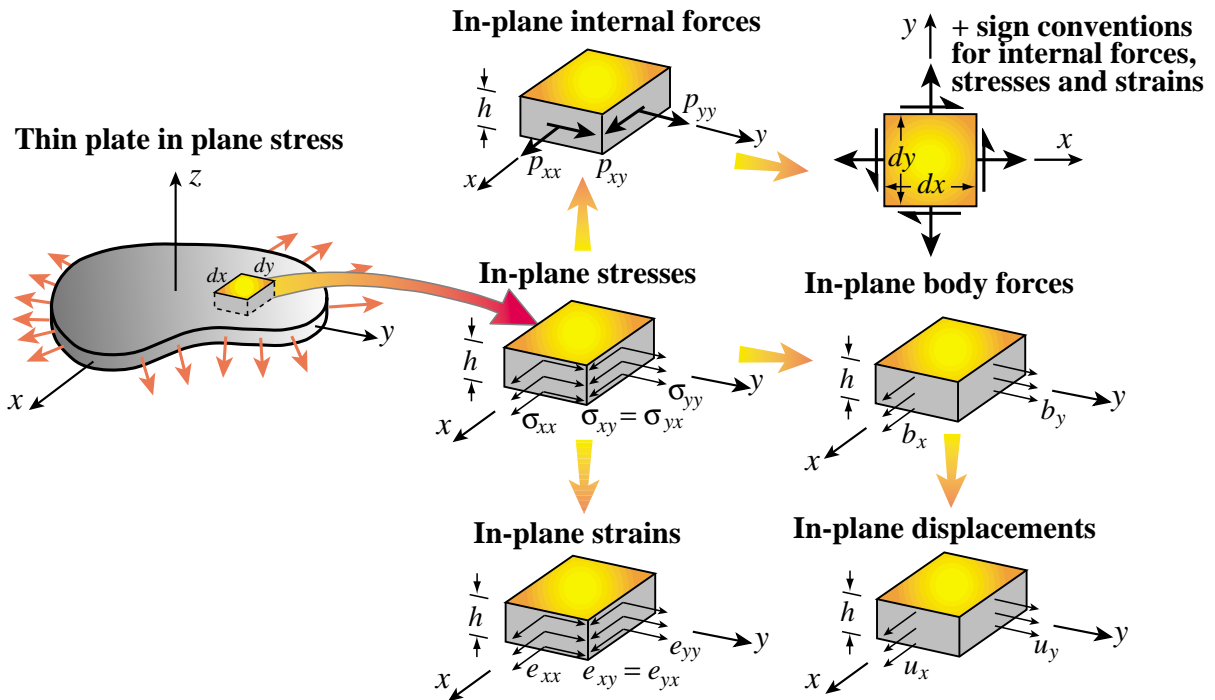


FIGURE 21.3. Notation for displacements, strains, stresses and forces in a thin plate in plane stress state.

### §21.2. Plate in Plane Stress

Several of the following examples pertain to a thin plate in a plane stress (also known as membrane) state. Notation and sign conventions for displacements, strains, stresses and forces in this mathematical model are collected in Figure 21.3. Assumptions associated with plane stress are discussed in detail in Chapter 14 of the Introduction to Finite Element Notes. Here we simply recall

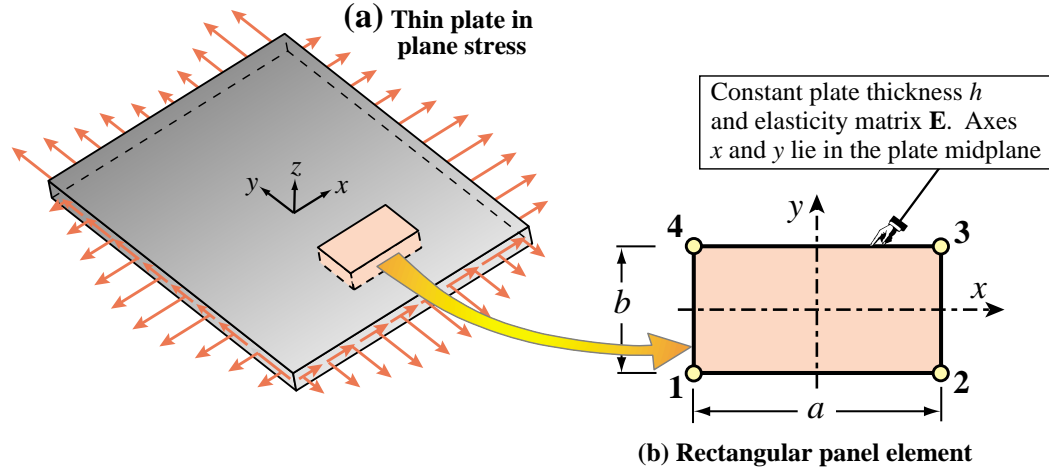


FIGURE 21.4. The four-node, 8DOF rectangular panel modeling a thin plate in plane stress.

the in-plane governing equations

$$\begin{aligned}
 \mathbf{e} &= \mathbf{D} \mathbf{u} \quad \text{or} \quad \begin{bmatrix} e_{xx} \\ e_{yy} \\ 2e_{xy} \end{bmatrix} = \begin{bmatrix} \partial/\partial x & 0 \\ 0 & \partial/\partial y \\ \partial/\partial y & \partial/\partial x \end{bmatrix} \begin{bmatrix} u_x \\ u_y \end{bmatrix}, \\
 \boldsymbol{\sigma} &= \mathbf{E} \mathbf{e} \quad \text{or} \quad \begin{bmatrix} \sigma_{xx} \\ \sigma_{yy} \\ \sigma_{xy} \end{bmatrix} = \begin{bmatrix} E_{11} & E_{12} & E_{13} \\ E_{12} & E_{22} & E_{23} \\ E_{13} & E_{23} & E_{33} \end{bmatrix} \begin{bmatrix} e_{xx} \\ e_{yy} \\ 2e_{xy} \end{bmatrix}, \\
 \mathbf{D}^T \boldsymbol{\sigma} + \mathbf{b} &= \mathbf{0} \quad \text{or} \quad \begin{bmatrix} \partial/\partial x & 0 & \partial/\partial y \\ 0 & \partial/\partial y & \partial/\partial x \end{bmatrix} \begin{bmatrix} \sigma_{xx} \\ \sigma_{yy} \\ \sigma_{xy} \end{bmatrix} + \begin{bmatrix} b_x \\ b_y \end{bmatrix} = \begin{bmatrix} 0 \\ 0 \end{bmatrix}.
 \end{aligned} \tag{21.1}$$

As regards stresses in the  $z$  direction, one assumes  $\sigma_{zz} = \sigma_{xz} = \sigma_{yz} = 0$ . The strains  $\{e_{zz}, e_{xz}, e_{yz}\}$  are determined from the three-dimensional strain-stress (compliance) constitutive equations. If the plate material is isotropic with elastic modulus  $E$  and Poisson's ratio  $\nu$ , the matrix constitutive equation  $\boldsymbol{\sigma} = \mathbf{E} \mathbf{e}$  and its inverse  $\mathbf{e} = \mathbf{E}^{-1} \boldsymbol{\sigma}$  become

$$\begin{bmatrix} \sigma_{xx} \\ \sigma_{yy} \\ \sigma_{xy} \end{bmatrix} = \frac{E}{1-\nu^2} \begin{bmatrix} 1 & \nu & 0 \\ \nu & 1 & 0 \\ 0 & 0 & \frac{1-\nu}{2} \end{bmatrix} \begin{bmatrix} e_{xx} \\ e_{yy} \\ 2e_{xy} \end{bmatrix}, \quad \begin{bmatrix} e_{xx} \\ e_{yy} \\ 2e_{xy} \end{bmatrix} = \frac{1}{E} \begin{bmatrix} 1 & -\nu & 0 \\ -\nu & 1 & 0 \\ 0 & 0 & 2(1+\nu) \end{bmatrix} \begin{bmatrix} \sigma_{xx} \\ \sigma_{yy} \\ \sigma_{xy} \end{bmatrix}. \tag{21.2}$$

For the isotropic case  $e_{xz} = e_{yz} = 0$ , whereas the thickness strain is

$$e_{zz} = -\frac{\nu}{E} (\sigma_{xx} + \sigma_{yy}) = -\frac{\nu}{1-\nu} (e_{xx} + e_{yy}). \tag{21.3}$$

### §21.3. Source Element 1: 4-node Rectangular Panel

The 4-node, 8-DOF rectangular element modeling a elastic thin plate in plate stress, sketched in Figure 21.4(a), is used as source element for the following examples. The element is called *rectangular panel* for brevity. As [] narrates, this is one of the two oldest continuum structural

elements, having been developed in the 1950s to model wing skin panels. This geometry is simple enough to be amenable to complete analytical development, but it is not trivial. Thus it provides a good illustration of the morphing process as well as of its strengths and pitfalls.

### §21.3.1. Rectangular Panel Template

The rectangular panel geometry is defined in Figure 21.4(b). Axes  $x$  and  $y$  are aligned with the sides for convenience. The element has constant thickness  $h$  and elasticity matrix  $\mathbf{E}$ . The 8 displacement degrees of freedom and associated node forces are collected in the vectors

$$\begin{aligned}\mathbf{u}_{RP} &= [u_{x1} \ u_{y1} \ u_{x2} \ u_{y2} \ u_{x3} \ u_{y3} \ u_{x4} \ u_{y4}]^T, \\ \mathbf{f}_{RP} &= [f_{x1} \ f_{y1} \ f_{x2} \ f_{y2} \ f_{x3} \ f_{y3} \ f_{x4} \ f_{y4}]^T.\end{aligned}\quad (21.4)$$

The element stiffness matrix may be expressed in template form as [refs] the sum of a *basic stiffness*  $\mathbf{K}_b$  and a *higher order stiffness*  $\mathbf{K}_h$ :

$$\begin{aligned}\mathbf{K} &= \mathbf{K}_b + \mathbf{K}_h = V \mathbf{H}_c^T \mathbf{E} \mathbf{H}_c + V \mathbf{H}_h^T \mathbf{W}^T \mathbf{R} \mathbf{W} \mathbf{H}_h, \\ \mathbf{H}_c &= \frac{1}{2ab} \begin{bmatrix} -b & 0 & b & 0 & b & 0 & -b & 0 \\ 0 & -a & 0 & -a & 0 & a & 0 & a \\ -a & -b & -a & b & a & b & a & -b \end{bmatrix}, \\ \mathbf{H}_h &= \frac{1}{2} \begin{bmatrix} 1 & 0 & -1 & 0 & 1 & 0 & -1 & 0 \\ 0 & 1 & 0 & -1 & 0 & 1 & 0 & -1 \end{bmatrix}, \\ \mathbf{W} &= \begin{bmatrix} 1/a & 0 \\ 0 & 1/b \end{bmatrix}, \quad \mathbf{R} = \begin{bmatrix} R_{11} & R_{12} \\ R_{12} & R_{22} \end{bmatrix}, \quad V = abh.\end{aligned}\quad (21.5)$$

Here  $R_{11}$ ,  $R_{12}$  and  $R_{22}$  are three free parameters with dimension of elastic moduli. The list  $\{R_{11}, R_{12}, R_{22}\}$  is called the *template signature*. All possible elements of this type that pass the Individual Patch Test (IET) of Bergan and Hanssen are instances of (21.5). Note that the basic stiffness  $\mathbf{K}_b$  is the same for all possible elements whereas the higher order stiffness  $\mathbf{K}_h$  depends on the signature  $\{R_{11}, R_{12}, R_{22}\}$ . The former specifies the element response to rigid body modes and constant strain states, whereas the latter characterizes the response to bending deformations. A particular template instance is defined by specifying its signature. Hence the only difference between elements of this type is their response to bending modes.

### §21.3.2. Morphing to Bar

The morphing of the rectangular panel to a 2-node, prismatic,  $x$ -aligned bar element is diagrammed in Figure 21.5. The  $x$  and  $y$  direction are called the *axial* and *transverse* directions, respectively. The material is assumed *isotropic*, obeying the constitutive equations (21.2). The target is the 2-node bar element shown in Figure 21.5(d), with node displacements and forces

$$\mathbf{u}_{bar} = \begin{bmatrix} u_{xi} \\ u_{xj} \end{bmatrix}, \quad \mathbf{f}_{bar} = \begin{bmatrix} f_{xi} \\ f_{xj} \end{bmatrix}.\quad (21.6)$$

The morphing process is carried out in two steps for convenience. First, the panel is assumed to deform symmetrically with respect to axes  $x$  and  $y$  placed along the rectangle medians, as sketched

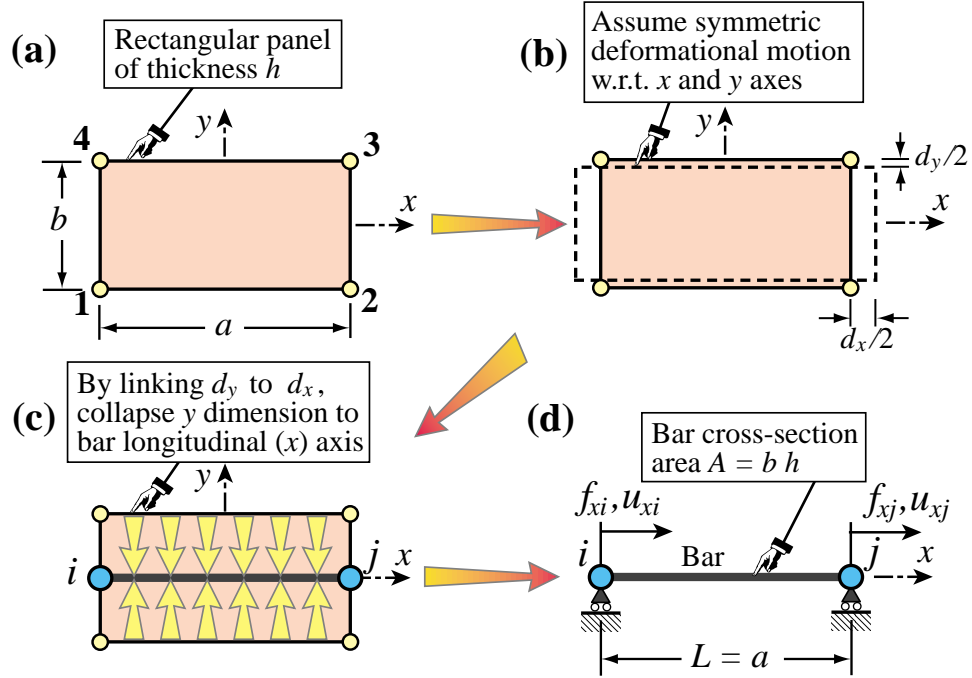


FIGURE 21.5. Morphing of the rectangular panel of Figure 21.4 (source element) to a 2-node prismatic bar element in the axial  $x$  direction.

in Figure 21.5(b). The axial and transverse elongations are called  $d_x$  and  $d_y$ , respectively, collected in array  $\mathbf{d}_{RP}$ . By inspection  $u_{x1} = u_{x4} = -\frac{1}{2}d_x$ ,  $u_{x2} = u_{x3} = \frac{1}{2}d_x$ ,  $u_{y1} = u_{y2} = -\frac{1}{2}d_y$  and  $u_{y3} = u_{y4} = \frac{1}{2}d_y$ . Those relations are collected in the transformation

$$\mathbf{u}_{RP} = \mathbf{T}_d \mathbf{d}_{RP} = \frac{1}{2} \begin{bmatrix} -1 & 0 & 1 & 0 & 1 & 0 & -1 & 0 \\ 0 & -1 & 0 & -1 & 0 & 1 & 0 & 1 \end{bmatrix}^T \mathbf{d}_{RP} \quad (21.7)$$

Applying (21.7) to the panel gives the deformational stiffness equations

$$\frac{E b h}{1 - \nu^2} \begin{bmatrix} \frac{1}{a} & \frac{\nu}{b} \\ \frac{\nu}{b} & \frac{a}{b^2} \end{bmatrix} \begin{bmatrix} d_x \\ d_y \end{bmatrix} = \frac{1}{2} \begin{bmatrix} f_{x2} + f_{x3} - f_{x1} - f_{x4} \\ f_{y3} + f_{y4} - f_{y1} - f_{y2} \end{bmatrix} = \begin{bmatrix} f_x \\ f_y \end{bmatrix}. \quad (21.8)$$

Note that the higher order stiffness parameters  $\{R_{11}, R_{12}, R_{22}\}$  are gone from (21.8) because  $\mathbf{H} \mathbf{T}_d = \mathbf{0}$ . Next, to get rid of the  $y$  dimension it is necessary to link  $d_y$  and  $d_x$ , bringing the 2D nature of the problem into play. If the  $y$  motion is unrestrained, Poisson's effect says that  $d_y = -\nu b d_x/a$ , which may also be obtained by solving the second of (21.8) for  $f_y = 0$ . On the other hand,  $d_y = 0$  if that motion is precluded. The degree of transverse restraint can be parametrized by taking  $d_y = -(1 - \alpha) \nu b d_x/a$ , where  $\alpha$  varies from 0 for unconstrained to 1 for fully constrained. Grouping that relation with  $d_x = u_{xj} - u_{xi}$  gives the transformation to the bar freedoms:

$$\mathbf{d}_{RP} = \mathbf{T}_b \mathbf{u}_{bar} = \begin{bmatrix} d_x \\ d_y \end{bmatrix} = \begin{bmatrix} -1 & 1 \\ \frac{(1 - \alpha) \nu b}{a} & -\frac{(1 - \alpha) \nu b}{a} \end{bmatrix} \begin{bmatrix} u_{xi} \\ u_{xj} \end{bmatrix}. \quad (21.9)$$

Applying (21.9) to (21.8) and replacing  $b h \rightarrow A$  and  $a \rightarrow L$  to pass to the more usual bar notation, gives the bar stiffness equations as

$$\frac{\hat{E} A}{L} \begin{bmatrix} 1 & -1 \\ -1 & 1 \end{bmatrix} \begin{bmatrix} u_{xi} \\ u_{yj} \end{bmatrix} = \begin{bmatrix} -f_x + \frac{(1-\alpha)\nu b}{L} f_y \\ f_x - \frac{(1-\alpha)\nu b}{L} f_y \end{bmatrix} = \begin{bmatrix} f_{xi} \\ f_{xj} \end{bmatrix}, \quad (21.10)$$

in which

$$\hat{E} = \frac{1 - (1 - \alpha^2)\nu^2}{1 - \nu^2} E. \quad (21.11)$$

is an effective axial modulus that reduces to  $E$  if either  $\nu = 0$  or  $\alpha = 0$ .

If the transformations in (21.7) and (21.9) are combined one gets

$$\mathbf{T}_{Rb} = \mathbf{T}_{Rd} \mathbf{T}_{db} = \frac{1}{2} \begin{bmatrix} 1 & -\frac{(1-\alpha)\nu b}{a} & -1 & -\frac{(1-\alpha)\nu b}{a} & -1 & \frac{(1-\alpha)\nu b}{a} & 1 & \frac{(1-\alpha)\nu b}{a} \\ 1 & \frac{(1-\alpha)\nu b}{a} & -1 & \frac{(1-\alpha)\nu b}{a} & -1 & -\frac{(1-\alpha)\nu b}{a} & 1 & -\frac{(1-\alpha)\nu b}{a} \end{bmatrix}^T. \quad (21.12)$$

Applying  $\mathbf{T}_{Rb}$  to the panel produces (21.10) in one shot, but the two-step morphing process is more illuminating. One could add rigid body motions of  $u_x = \frac{1}{2}$  and  $u_y = \frac{1}{2}$  to the 2 columns of  $\mathbf{T}_{Rb}$ , respectively, to produce more zero entries but the morphed bar equation would be the same.

The corresponding process for the non-isotropic case, which is not covered here, is more involved unless material tensor symmetries allow symmetries to be introduced in the first step. Otherwise one has to start with uniform stress assumptions, convert to strains, integrate for displacements and evaluate at nodes.

### §21.3.3. Morphing to Simply Supported Beam

We next consider morphing to a prismatic, 2-node, simply-supported,  $x$  aligned beam element as diagrammed in Figure 21.6. The material is assumed to be isotropic. The target is the 2-node Bernoulli-Euler beam element shown in Figure 21.6(d), with node displacements and forces

$$\mathbf{u}_{beam} = \begin{bmatrix} \theta_{zi} \\ \theta_{zj} \end{bmatrix}, \quad \mathbf{f}_{beam} = \begin{bmatrix} M_{zi} \\ M_{zj} \end{bmatrix}. \quad (21.13)$$

Here  $\theta_z$  is the cross section rotation about  $z$ , positive CCW and  $M_z$  the corresponding generalized force. The element can take only a constant bending moment. As in the previous example the process is carried out in two steps. First the deformational motion sketched in Figure 21.6(b) is assumed. This motion is symmetric about  $y$  and antisymmetric about  $x$ . Deformational displacements  $d_x$  and  $d_y$  are defined in that figure. The resulting freedom transformation is

$$\mathbf{u}_{RP} = \mathbf{T}_d \mathbf{d}_{RPbend} = \frac{1}{2} \begin{bmatrix} -1 & 0 & 1 & 0 & -1 & 0 & 1 & 0 \\ 0 & 1 & 0 & 1 & 0 & 1 & 0 & 1 \end{bmatrix}^T \begin{bmatrix} d_x \\ d_y \end{bmatrix}. \quad (21.14)$$

The transformed stiffness equations are

$$\frac{bh R_{11}}{a} \begin{bmatrix} 1 & 0 \\ 0 & 0 \end{bmatrix} \begin{bmatrix} d_x \\ d_y \end{bmatrix} = \frac{1}{2} \begin{bmatrix} f_{x2} - f_{x3} - f_{x1} + f_{x4} \\ f_{y1} + f_{y2} + f_{y3} + f_{y4} \end{bmatrix} = \begin{bmatrix} f_x \\ f_y \end{bmatrix}. \quad (21.15)$$

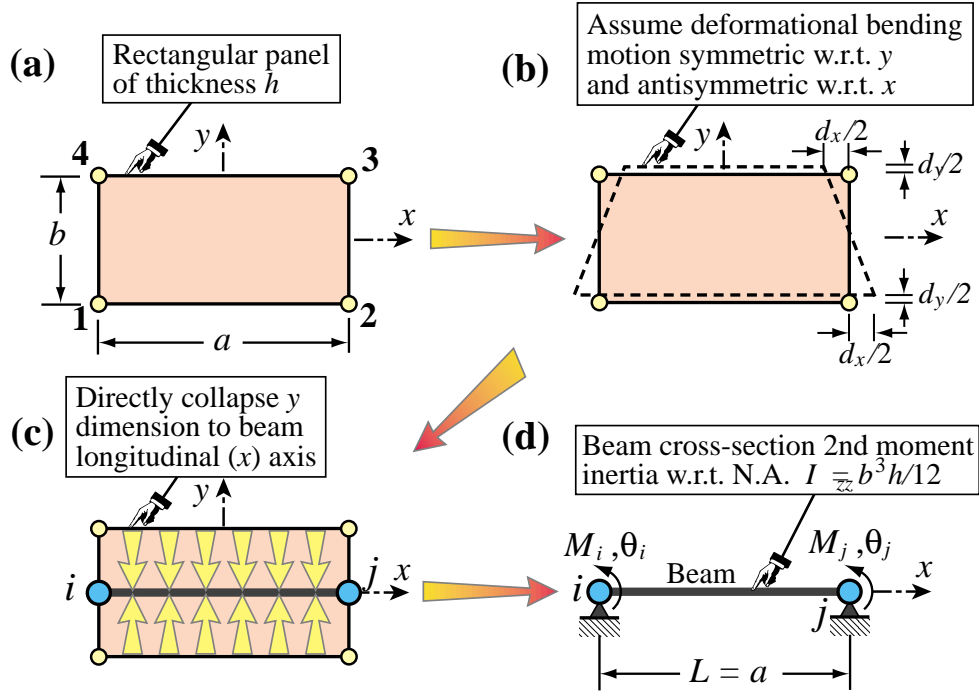


FIGURE 21.6. Morphing of the rectangular panel of Figure 21.4 (source element) to a 2-node, prismatic, simply-supported Bernoulli-Euler beam element in the axial  $x$  direction.

Although the transverse ( $y$ ) motion pictured in Figure 21.6(b) is deformational, arising from Poisson's ratio effects, it appears as a  $y$  rigid body to the panel freedoms since  $u_{y1} = u_{y2} = u_{y3} = u_{y4} = \frac{1}{2}d_y$ . This explains the disappearance of  $d_y$  in (21.15). The  $x$  deformation  $d_x$  may be expressed in term of beam rotational DOF as  $d_x/2 = (\theta_{zj} - \theta_{zi}) b/2$ , or in matrix form

$$\mathbf{d}_{SSbeam} = [d_x] = [-1 \quad 1] \begin{bmatrix} \theta_{zi} \\ \theta_{zj} \end{bmatrix} = \mathbf{T}_{db} \boldsymbol{\theta}. \quad (21.16)$$

Transforming (21.15) as per (21.16), and setting  $\frac{1}{12}b^3 h \rightarrow I_{zz}$  and  $a \rightarrow L$  to pass to standard beam notation, yields

$$\frac{4R_{11} I_{zz}}{3L} \begin{bmatrix} 1 & -1 \\ -1 & 1 \end{bmatrix} \begin{bmatrix} \theta_{xi} \\ \theta_{yj} \end{bmatrix} = \frac{1}{2}b \begin{bmatrix} f_{x1} - f_{x2} + f_{x3} - f_{x4} \\ -f_{x1} + f_{x2} - f_{x3} + f_{x4} \end{bmatrix} = \begin{bmatrix} M_{zi} \\ M_{zj} \end{bmatrix}. \quad (21.17)$$

To make (21.17) agree with the correct Bernoulli-Euler beam stiffness equations, it is necessary to take

$$R_{11} = \frac{1}{3}E. \quad (21.18)$$

This result was established in [1] with other methods. The anisotropic case is treated there.

### §21.3.4. Morphing to Spar

We next consider morphing to a prismatic, 2-node,  $x$  aligned spar element as diagrammed in Figure 21.7. The material is assumed to be isotropic. The target is the 2-node spar element shown

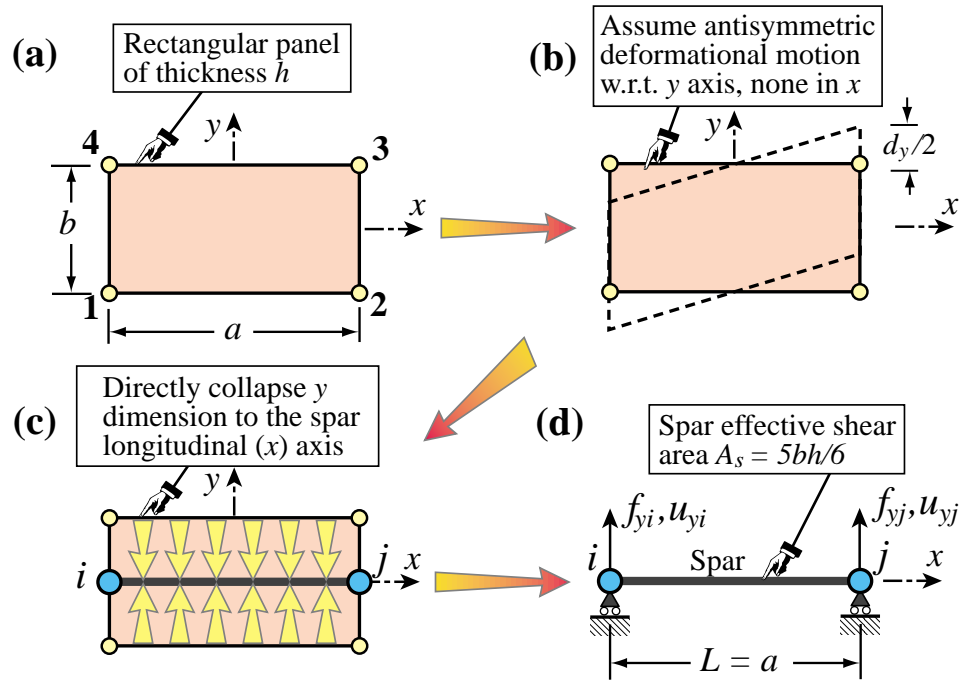


FIGURE 21.7. Morphing of the rectangular panel of Figure 21.4 (source element) to a 2-node, prismatic, spar element in the axial  $x$  direction.

in Figure 21.6(d), with node displacements and forces

$$\mathbf{u}_{spar} = \begin{bmatrix} u_{yi} \\ u_{yj} \end{bmatrix}, \quad \mathbf{f}_{spar} = \begin{bmatrix} f_{yi} \\ f_{yj} \end{bmatrix}. \quad (21.19)$$

The spar element can take only a constant shear force. As in the previous 2 examples the process is carried out in two steps. First the deformational motion sketched in Figure 21.7(b) is assumed. This motion is antisymmetric about  $y$  and zero along  $x$ , since the element deforms only in shear. The deformational displacement  $d_y$  is defined in that figure. The resulting freedom transformation is

$$\mathbf{u}_{RP} = \mathbf{T}_d \mathbf{d}_{RPspar} = \frac{1}{2} [0 \quad -1 \quad 0 \quad 1 \quad 0 \quad 1 \quad 0 \quad -1]^T [d_y]. \quad (21.20)$$

The transformed stiffness equations are

$$\frac{Eb}{2(1+\nu)a} [1] [d_y] = \frac{1}{2} [f_{y2} + f_{x3} - f_{x1} - f_{y4}] = [f_x]. \quad (21.21)$$

The deformation  $d_y$  may be expressed in term of spar translations

$$[d_y] = [-1 \quad 1] \begin{bmatrix} u_{yi} \\ \theta_{yj} \end{bmatrix} = \mathbf{T}_{ds} \mathbf{u}_{spar}. \quad (21.22)$$

Applying this transformation, and passing to the usual spar element notation:  $E/(2(1+\nu)) \rightarrow G$ ,  $bh \rightarrow A$ ,  $a \rightarrow L$ , gives

$$\frac{GA}{L} \begin{bmatrix} 1 & -1 \\ -1 & 1 \end{bmatrix} \begin{bmatrix} u_{yi} \\ u_{yj} \end{bmatrix} = \begin{bmatrix} f_{yi} \\ f_{yj} \end{bmatrix}. \quad (21.23)$$

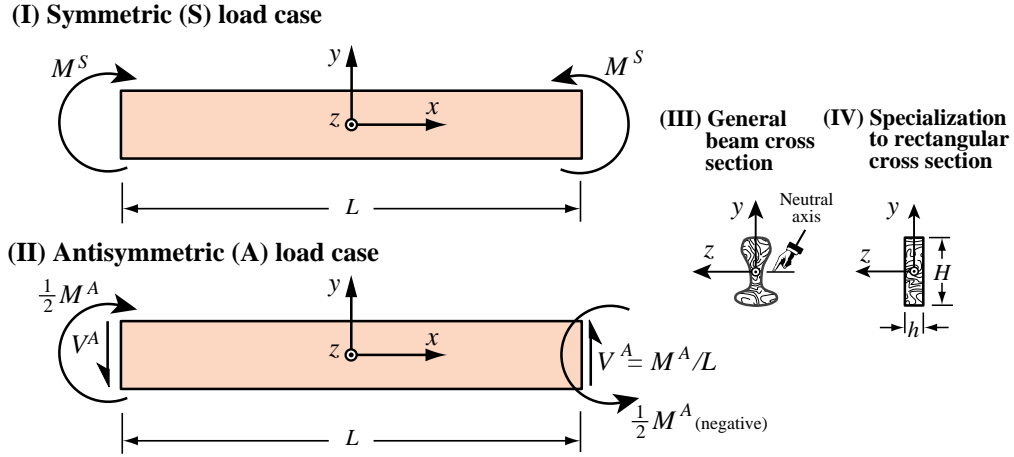


FIGURE 21.8. Benchmark beam solution used for advanced morphing examples.

The result (21.23) agrees with the spar stiffness equations derived with Mechanics of Materials methods (for example, in Chapter 5 of the Introduction to Finite Elements Notes) except for one detail: the transverse panel area  $A = bh$  should be replaced by the effective shear area. For a narrow rectangle with  $h \ll b$ ,  $A_s = 5bh/6$ . This discrepancy does not reflect, however, a flaw in the source element. The parabolic shear stress distribution that produces that  $A_s$  assumes that  $\sigma_{xy}$  vanishes at the top and bottom spar surfaces  $y = \pm \frac{1}{2}b$ . This will not generally be the case when the panel is used in a 2D mesh.

### §21.4. Benchmark Plane Beam Solutions

To support more advanced morphing examples it is convenient to have a benchmark beam solution that is exact in the sense of plane stress isotropic elasticity, as well as that provided by the shear-flexible Timoshenko beam model. The problem is illustrated in Figure 21.8. The beam has span  $L$  and prismatic cross section. Axes  $\{x, y, z\}$  are chosen as shown. Equations are initially derived for a general cross section sketched in Figure 21.8(III) and later specialized to the rectangular cross section of height  $H$  and width  $h$  illustrated in Figure 21.8(IV). For a general cross section, the moment of inertia with respect to the neutral axis  $z$  is  $I_{zz}$ , the cross section area is  $A$ . The internal bending moment is  $M_z$  and the transverse (resultant) shear force is  $V_y$ , with the usual sign conventions.

The material is isotropic with elastic modulus  $E$ , shear modulus  $G$  and Poisson's ratio  $\nu$  and shear modulus  $G = E/(2(1 + \nu))$ . The in-plane displacements are  $\{u_x, u_y\}$  and the infinitesimal rotation about  $z$  is  $\theta_z = \frac{1}{2}(\partial u_y/\partial x - \partial u_x/\partial y)$ . The effective shear area is  $A_s = k_s A$ , in which  $k_s$  is Timoshenko's static shear correction coefficient defined by<sup>1</sup>

$$U_S \stackrel{\text{def}}{=} \frac{1}{2} \int_V \frac{V_y^2}{G A_s} dV = \frac{1}{2} \int dx \int \frac{V_y^2}{G k_s A} dA, \tag{21.24}$$

in which  $U_S$  is the internal energy due to transverse shear stresses. The following symbols are introduced for later use:

$$r_{Gz}^2 = \frac{I_{zz}}{A}, \quad \Phi = \frac{12 E I_{zz}}{G A_s L^2} = \frac{12 E r_{Gz}^2}{G k_s L^2} = \frac{24(1 + \nu) r_{Gz}^2}{k_s L^2}. \tag{21.25}$$

<sup>1</sup> Some authors use the inverse value: e.g.,  $k = 1/k_s$  in [34, p. 177] and  $m = 1/k_s$ . in [18, p. 21].

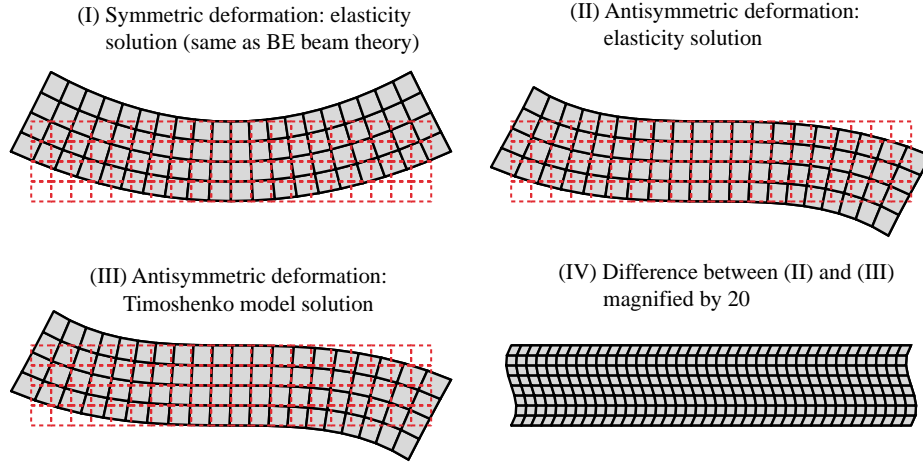


FIGURE 21.9. Deformed shapes for benchmark solutions. Beam of rectangular cross section with  $L = 5$ ,  $H = 2$ ,  $h = 1$ ,  $E = 1$ ,  $\nu = 1/4$ ,  $\kappa_S = 1$  and  $\kappa^A = 3$ .

Here  $r_{Gz}$  denotes the radius of gyration of the cross section about the neutral axis  $z$  while  $\Phi$  is a dimensionless measure of the section-averaged shear rigidity of the element, which is used in the Timoshenko model. The last form of  $\Phi$  given in (21.25) assumes an isotropic material.

Two load systems pictured in Figure 21.8(I,II) are considered:

- (S) Symmetric: pure bending produced by equal and opposite applied end moments  $M^S$ . The bending moment  $M_z = M_{z,S}$  is constant along the beam whereas the transverse shear force  $V_y$  is zero.
- (A) Antisymmetric: linearly varying bending produced by equal and opposite shear forces  $V^A$  balanced by end moments with total resultant  $M^A = V_y L$ . The internal bending moment  $M_z = -M^A x/L$  varies linearly from  $+\frac{1}{2}M^A$  at  $x = -\frac{1}{2}L$  through  $-\frac{1}{2}M^A$  at  $x = \frac{1}{2}L$ . The transverse shear force  $V_y$  is constant and equal to  $V^A$ .

### §21.4.1. Symmetric Solution

The symmetric displacement solution is

$$u_x^S = -\kappa_S x y, \quad u_y^S = \frac{1}{2} \kappa_S (x^2 + y^2 \nu), \quad \theta_z^S = \frac{1}{2} \left( \frac{\partial u_y^S}{\partial x} - \frac{\partial u_x^S}{\partial y} \right) = \kappa_S x. \quad (21.26)$$

in which  $\kappa_S = M_z^S / (EI_{zz}) = \partial^2 u_y^S / \partial x^2$  is the constant curvature produced by  $M^S$ . The deformed shape, pictured in Figure 21.9(I), is symmetric about  $x$  and  $y$ . The associated strains and stresses are

$$e_{xx}^S = -\kappa_S y, \quad e_{yy}^S = -\nu e_{xx}^S, \quad \gamma_{xy}^S = 0, \quad \sigma_{xx}^S = -E \kappa_S y, \quad \sigma_{yy}^S = 0, \quad \sigma_{xy}^S = 0. \quad (21.27)$$

The stresses (21.27) satisfy identically the plane stress differential equilibrium equations for any plane-symmetric cross section. The internal energy stored in the beam is

$$U = \frac{1}{2} \int_V \sigma_{xx} e_{xx} dV = \frac{1}{2} E L \kappa_S^2 \int_A y^2 dA = \frac{1}{2} E I_{zz} \kappa_S^2 L = \frac{1}{2} M^S \kappa_S L. \quad (21.28)$$

### §21.4.2. Antisymmetric Elasticity Solution

The antisymmetric displacement solution for an elastic isotropic material is

$$\begin{aligned} u_x^A &= \frac{\kappa_A y}{6L} (3x^2 - y^2(2 + \nu) + 18r_{Gz}^2(1 + \nu)), \\ u_y^A &= -\frac{\kappa_A x}{6L} (x^2 + 3\nu y^2), \quad \theta_z^A = -\frac{\kappa_A}{2L} ((x^2 - y^2) + 3r_{Gz}^2(1 + \nu)) \end{aligned} \quad (21.29)$$

The deformed shape is pictured in Figure 21.9(II) for a rectangular cross section with the values given there. The associated strains and stresses are

$$\begin{aligned} e_{xx}^A &= \frac{\kappa_A}{L} x y, \quad e_{yy}^A = -\nu e_{xx}^A, \quad \gamma_{xy}^A = \frac{\kappa_A(1 + \nu)}{L} (3r_{Gz}^2 - y^2), \\ \sigma_{xx}^A &= E \frac{\kappa_A}{L} x y, \quad \sigma_{yy}^A = 0, \quad \sigma_{xy}^A = E \frac{\kappa_A}{2L} (3r_{Gz}^2 - y^2) \end{aligned} \quad (21.30)$$

It is easily verified that  $\int_A \sigma_{xx}^A dA = E I_{zz} \kappa_A (x/L) = M^A$ . To show that  $\int_A \sigma_{xy}^A dA = V^A$ , integrate over  $A$ , use  $I_{zz} = \int_A y^2 dA = A r_{Gz}^2$  and  $V^A = M^A/L = E I_{zz} \kappa_A/L$ . The elasticity equilibrium equations are also satisfied identically. As regards stress boundary conditions, note that  $\sigma_{xy}^A$  vanishes at  $y = \pm\sqrt{3}r_{Gz}$ . These are not the top and bottom beam fibers unless the cross section is rectangular.

### §21.4.3. Antisymmetric Timoshenko Solution

The solution provided by the Timoshenko beam model, which assumes a constant average shear over the cross section is

$$\begin{aligned} u_x^{Timo} &= \frac{\kappa_A y}{6L} (3x^2 + \nu y^2 + 12r_{Gz}^2(1 + \nu)), \\ u_y^{Timo} &= -\frac{\kappa_A x}{6L} (x^2 + 3\nu y^2), \quad \theta_z^{Timo} = -\frac{\kappa_A}{2L} (x^2 + \nu y^2 + 2r_{Gz}^2(1 + \nu)) \end{aligned} \quad (21.31)$$

The deformed shape is pictured in Figure 21.9(III) for a rectangular cross section with the same values used for (II). There is no discernible difference between the elasticity and Timoshenko solutions at the plot scaled used there. The difference is shown Figure 21.9(IV) with displacements magnified by 20. While vertical displacements are the same, the elasticity solution accounts for the warping of the cross sections:  $u_x^A - u_x^{Timo} = \kappa_A y (1 + \nu)(2r_{Gz}^2 - y^2)/2L$ . The associated strains and stresses are

$$\begin{aligned} e_{xx}^{Timo} &= \frac{\kappa_A}{L} x y, \quad e_{yy}^{Timo} = -\nu e_{xx}^{Timo}, \quad \gamma_{xy}^{Timo} = 2\frac{\kappa_A}{L} r_{Gz}^2 (1 + \nu), \\ \sigma_{xx}^{Timo} &= E \frac{\kappa_A}{L} x y, \quad \sigma_{yy}^{Timo} = 0, \quad \sigma_{xy}^{Timo} = E \frac{\kappa_A}{L} r_{Gz}^2. \end{aligned} \quad (21.32)$$

### §21.4.4. Specialization to a Rectangular Cross Section

For the  $H \times h$  rectangular cross section,  $A = Hh$ ,  $I_{zz} = H^3 h/12$ ,  $r_{Gz}^2 = H^2/12$ ,

$$\begin{aligned} u_x^S &= -\kappa_S x y, \quad u_y^S = \frac{1}{2}\kappa_S (x^2 + \nu y^2), \quad \theta_z^S = \kappa_S x, \\ u_x^A &= \frac{\kappa_A y}{L} (x^2 - \frac{2+\nu}{3}y^2 + \frac{1+\nu}{3}H^2), \quad u_y^A = -\frac{\kappa_A x}{3L} (x^2 + 3\nu y^2), \quad \theta_z^A = -\frac{\kappa_A}{L} ((x^2 - y^2) + \frac{1+\nu}{6}H^2) \\ u_x^{AT} &= \frac{\kappa_A y}{L} (x^2 + \frac{\nu}{3}y^2 + \frac{1+\nu}{3}H^2), \quad u_y^{AT} = -\frac{\kappa_A x}{3L} (x^2 + 3\nu y^2), \quad \theta_z^{AT} = -\frac{\kappa_A}{L} ((x^2 + \nu y^2) + \frac{1+\nu}{6}H^2). \end{aligned} \quad (21.33)$$